Journal of
Materials Chemistry B

Materials for biology and medicine

Accepted Manuscript

This article can be cited before page numbers have been issued, to do this please use: G. Schwarz and J. L. Holloway, *J. Mater. Chem. B*, 2025, DOI: 10.1039/D5TB00694E.

ROYAL SOCIETY OF CHEMISTRY

rsc.li/materials-b

View Article Online
DOI: 10.1039/D5TB00694E

Temporal and Spatial Control Over Fiber Alignment Within Hyaluronic Acid Hydrogels Using Magnetic Fields

Grace Schwarz,[a] Julianne L. Holloway[ab*]

[a]Biological Design, School for Engineering of Matter, Transport and Energy, Arizona State University, Tempe, Arizona, 85287, United States

[b]Chemical Engineering, School for Engineering of Matter, Transport and Energy, Arizona State University, Tempe, Arizona, 85287, United States

*Corresponding Author: Julianne L. Holloway (Julianne.Holloway@asu.edu)

Abstract

Wound healing is tightly regulated in both space and time. To mimic this behavior, we designed magnetically-responsive, fiber-hydrogel composites. When covalently crosslinked hydrogels were combined with layer-by-layer stacking, we demonstrated precise spatial control over fiber orientation. For temporal control, we used non-covalently crosslinked hydrogels to enable in situ fiber alignment.

Keywords

Magnetically-responsive; hydrogels; composites; spatial control; temporal control; fibers

View Article Online
DOI: 10.1039/D5TB00694E

Introduction

There are 14 million fibrous connective tissue injuries annually in the United States.(1) Fibrous connective tissues are highly organized tissues like ligaments, tendons, and joint capsules.(1) Healing of fibrous connective tissue injuries often deposits dense, disorganized tissue instead of healthy, organized tissue, resulting in altered mechanotransduction and ultimately reducing the tissue's function.(1,2) Tissue engineering is a maturing scientific field where cells, scaffolds, and biomolecules are combined to improve healing outcomes.(2–5) The three stages of healing are inflammation, proliferation, and remodelling.(6) Each stage has unique chemical and physical signalling.(7) In the inflammation stage, the inflammatory response is triggered, clots are formed, and signalling cues are released to trigger the migration of cells required for the proliferation stage. In the proliferation stage, cells migrate to the wound area, undergo proliferation, and deposit a disorganized collagen matrix. In the remodelling stage, the collagen matrix is remodelled into a more organized structure.(4,6) Fiber organization is essential for the formation of healthy, functional tissue; however, the temporal role of fibrous cues during this healing response is not well understood. Thus, there is a need to develop new biomaterial platforms that enable dynamic, three-dimensional (3D) control over fibrous cues to investigate the temporal and spatial role of these biophysical signals on cell behavior.

Fibrous-based scaffolds are commonly fabricated using electrospinning, a widely used and well understood technique.(4,5,8,9) Electrospinning allows users to easily tailor the process parameters to create fibrous mats with physical cues that closely mimic the fiber diameter, alignment, nanotopography, and more, of the extracellular matrix (ECM).(4,5,8–12) These physical cues have been shown to significantly influence cell adhesion, migration, and differentiation.(2,4,5,9) Nonetheless, electrospun scaffolds can be very dense, inhibiting cell migration into the scaffold interior, and it remains challenging to spatially and temporally control scaffold properties in 3D.
To address this challenge, researchers have investigated sophisticated fiber synthesis methods, like single-needle blend electrospinning(11) and heparin-driven self-assembly,(13) to create stimuli-responsive fibers. Additionally, electrospun fibers can be encapsulated in hydrogels to form composite biomaterials that can be molded into user-defined 3D geometries while still providing physical cues that mimic ECM architecture.(14–16) Composite biomaterials are often designed to combine the advantages of their constituent parts, increasing the functionality of the material.(15) When stimuli-responsive fibers are combined with hydrogels, this creates a fiber-hydrogel composite that can dynamically respond to the environment through softening,(16) molecule release,(17) reversible superstructures,(18) and reversible shape-morphing.(19) The inclusion of fibers within fiber-hydrogel composites has been shown to promote cell spreading and is essential for long-range force transmission.(20,21) The biomaterials field has begun to utilize fiber-hydrogel composites more frequently; nonetheless, none of these systems are capable of spatially and temporally controlling fiber organization in 3D.

To address this knowledge gap, this work combines magnetically-responsive fibers within a hyaluronic acid hydrogel to enable spatial and temporal control over 3D fiber alignment. Electrospun fibers were fabricated with encapsulated superparamagnetic iron oxide nanoparticles (SPIONs) to enable user-controlled fiber alignment via magnetic field application. Hyaluronic acid (HA) was selected for the hydrogel component due to its biological relevance and ease of chemical modification.(22) To enable spatial control, norbornene-functionalized HA (NorHA) was used for the fiber-hydrogel composite.

View Article Online
DOI: 10.1039/D5TB00694E

NorHA can be covalently crosslinked with UV light to form a hydrogel and layer-by-layer stacking can be used to create a multi-layered hydrogel with distinct properties in each layer.(3,23) With this technique, fiber alignment was independently controlled via magnetic field application within each hydrogel layer and alignment was locked in place following hydrogel crosslinking. To enable temporal control, guest-host chemistry was used for the hydrogel component of the composite. Specifically, adamantine-modified HA (Ad-HA, guest) was combined with cyclodextrin-modified HA (CD-HA, host) to form a guest-host complex. This complex forms due to hydrophobic interactions between adamantine and cyclodextrin and serves as a non-covalent crosslink. These dynamic bonds can be easily broken via force application (shear-thinning) and repaired following force removal (self-healing).(24) The shear-thinning and self-healing behavior of these materials was leveraged to enable temporal control over fiber alignment upon magnetic field application.

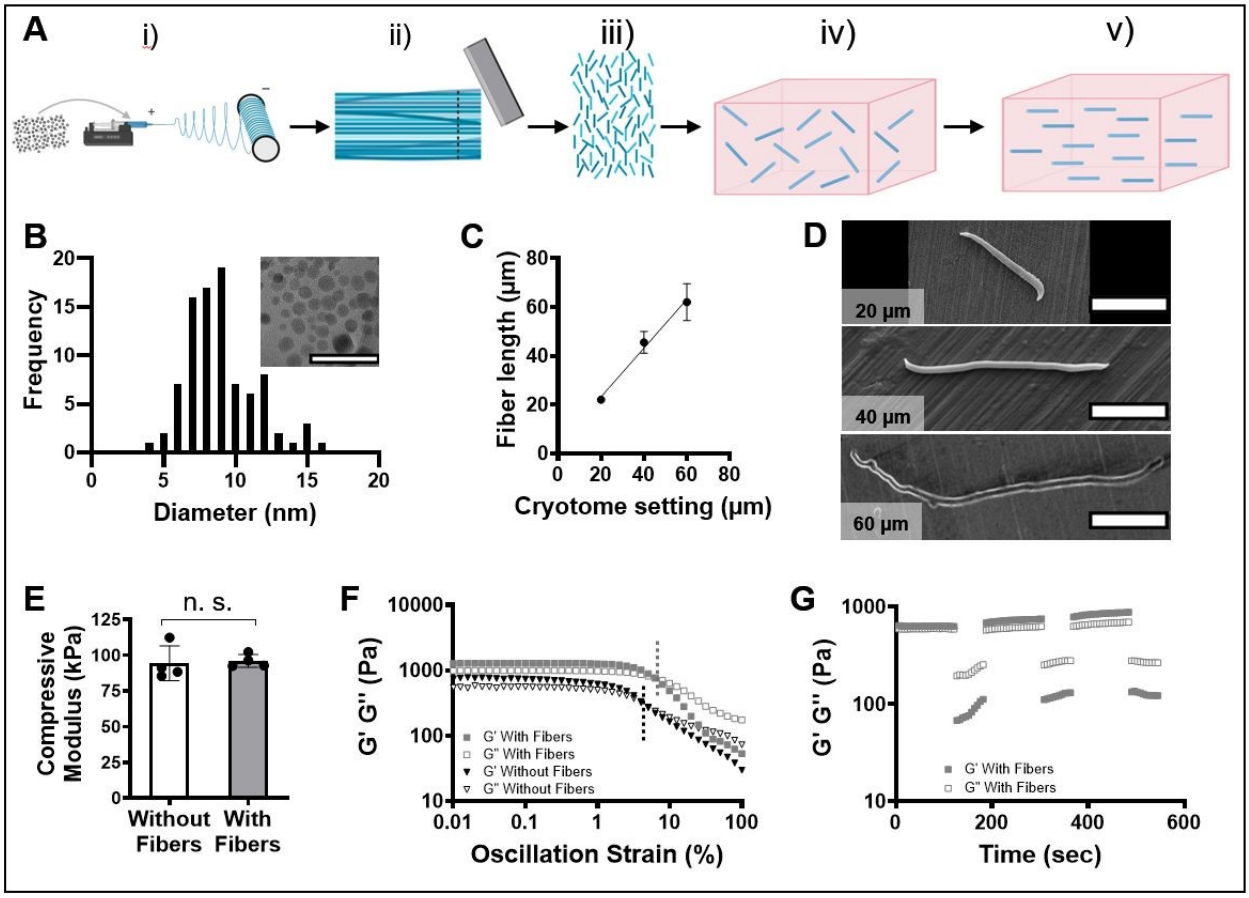

Figure 1. Fabrication and characterization of magnetically-responsive, fiber-hydrogel composites. A) Schematic of magnetically-responsive, fiber-hydrogel manufacturing process. (i) Magnetic nanoparticles were dispersed into a solution and electrospun, (ii) the mat was chopped into fibers, (iii) which were washed (iv) before encapsulation in the polymer solution/hydrogel and (v) exposed to an external magnetic field to align the fibers within the polymer solution/hydrogel (created with BioRender.com). B) Distribution of SPIONs as a function of diameter with representative TEM image of SPIONs (inset). Scale bar is 50 nm. C) Chopped fiber length as a function of cryotome setting. D) SEM images of 20, 40, and 60 μm fibers. Scale bar is 10 μm. E) Compressive modulus of the covalently-crosslinked hydrogel with and without fibers, n. s. indicates no statistical significance. Storage modulus (G', closed markers) and loss modulus (G", open markers) of the non-covalently crosslinked hydrogel during a F) strain sweep (dashed vertical lines indicate the crossover strain) or G) cyclic strain time sweep with alternating periods of low (0.2%) and high (100%) strain.

View Article Online
DOI: 10.1039/D5TB00694E

Results and Discussion

Fiber-hydrogel composites were synthesized using the following general steps: (i) magnetic nanoparticles were dispersed into a polymer solution and electrospun, (ii) the fibrous mat was chopped into short fibers, (iii) which were washed (iv) before encapsulation in the polymer solution/hydrogel and (v) exposed to an external magnetic field to align the fibers within the polymer solution/hydrogel (**Figure 1A**). To create magnetically-responsive fibers, we first synthesized SPIONs using a two-step reaction as described by Bloemen, 2012.(31) Iron oleate was synthesized and then thermally decomposed to form SPIONs coated with oleic acid, to enable dispersion in the electrospinning solution. Superparamagnetism is a size-dependent form of magnetism where a particle under 20 nm can exhibit high magnetic susceptibility while maintaining a coercivity close to zero.(25) Superparamagnetic particles respond strongly to an external magnetic field while lacking a meaningful magnetic field of their own. Using SPIONs instead of a larger magnetic particle enables the same magnetic responsiveness with a much lower volume of iron oxide, reducing toxicity concerns.(14,26–28) SPIONs were analyzed using transmission electron microscopy (TEM, JEOL 2010F) to measure particle size. The synthesis resulted in particles with an average diameter of 9.5 nm ± 2.4 nm (**Figure 1B**), well below the threshold for superparamagnetism.

Next, magnetically responsive fibers were fabricated using a procedure adapted from Omidinia-Anarkoli, 2017.(14) In short, an aligned fibrous mat was created by electrospinning a solution containing 17 wt% polycaprolactone (80 kDa) dissolved in 1:1 chloroform:acetic acid with 0.25 wt% Nile Red for visualization and either 5, 10, or 15 wt% SPIONs. The electrospinning solution was expelled at a rate of 1.5 mL/hr with a positive voltage of 6-12 kV at a needle to collector distance of 16 cm onto a cylindrical mandrel rotating at 10 m/s with a negative voltage of 0.9-2.3 kV. The aligned fiber mat was coated in Tissue-Tek and frozen. The frozen mat was cut and stacked, maintaining fiber alignment, placed into a mold, then the mold was filled with Tissue-Tek and frozen again. The resultant block of fibers was sliced to the desired length using a cryostat. Researchers have evaluated the use of many different fiber lengths within fiber-hydrogel composites, where there is a trade-off between maintaining a high aspect ratio and avoiding physical entanglement.(2,14) For this work, the fibers must be long enough to direct cellular extension along an axis,(29) yet small enough to align within a reasonable timespan and under a reasonable magnetic field strength.(15,30,31) Given these considerations, we selected fiber lengths of 20, 40, and 60 μm and magnetic field strengths between 300-760 mT, which is less than the typical field strength used during clinical magnetic resonance imaging (MRI).(32) Here, fiber length was well-controlled by adjusting the cryostat settings. The ’20 μm’, ’40 μm’, and ’60 μm’ setting on the cryostat resulted in fibers of 22.0 ± 1.5 μm, 45.6 ± 4.5 μm, and 62.1 ± 7.6 μm in length, respectively (**Figure 1C**). Chopped fibers were washed using phosphate buffered saline (PBS), filtered through a 25 μm mesh, condensed into a single pellet via centrifugation, and dried. Dried chopped fibers were stored at room temperature and protected from light. Dried fibers were imaged using scanning electron microscopy (**Figure 1D, S1**) (SEM, Nova 200 NanoLab SEM/Focused Ion Beam). Images were captured at 5.0 kV using a magnification between 150X and 25,000X. ImageJ was used to quantify fiber length. Dried fibers were dispersed at 0.5 wt% in PBS via overnight mixing on a shaker before use. Fibers in PBS rapidly aligned in the presence of a magnetic field, demonstrating magnetic responsive behavior (**Supplementary Video 1**).

To fabricate covalently crosslinked fiber-hydrogel composites, norbornene-functionalized HA (NorHA) was synthesized using a two-step reaction as previously published.(23)

View Article Online
DOI: 10.1039/D5TB00694E

NorHA was purified via dialysis, lyophilized, frozen for storage, and functionalization was determined via ^{1}H NMR. Norbornene functionalization of HA was calculated as the area of four vinyl proton peaks from 6.02-6.33 ppm (2H), normalized to the methyl peak along the HA backbone at 2.1 ppm (3H).(23,33) Approximately 80% of the disaccharide repeat units within HA were modified with norbornenes (**Figure S2**). NorHA (4 wt%) was dissolved in PBS containing 0.5 wt% fibers, 0.05 wt% I2959 (photoinitiator), and dithiothreitol (crosslinker, 0.2:1 molar ratio of thiol to norbornene). The polymer solution was pipetted into a custom mold and fibers were aligned within the solution by applying a magnetic field using two neodymium magnets at 37°C. The magnetic field strength was controlled by adjusting the distance between the two magnets and measured using a magnetometer. After a specified amount of time, the hydrogel was crosslinked using UV light (10 mW/cm^2) for 5 minutes. The crosslinking time was based on previous studies which demonstrated hydrogel modulus reached a plateau within 5 minutes of UV light exposure, indicative of complete crosslinking.(34) Mechanical analysis of the NorHA hydrogels, with and without fibers, was performed via uniaxial compression testing (Instron 5943, 50 N load cell). Testing was performed at 100% strain/min until 15% strain and the compressive modulus was calculated as the initial linear region of the stress versus strain curve. NorHA hydrogels with and without fibers had a compressive modulus of 95.9 ± 4.5 kPa and 94.3 ± 12.2 kPa, respectively. Thus, the inclusion of fibers did not appear to inhibit crosslinking or significantly impact the compressive modulus of NorHA hydrogels (**Figure 1E**). At a relatively low fiber density of 0.5 wt%, the fibers were not expected to alter the material's compressive properties.(2)

To fabricate non-covalently crosslinked fiber-hydrogel composites, Ad-HA and CD-HA were synthesized using previously published protocols.(24) Ad-HA and CD-HA were purified via dialysis, lyophilized, frozen for storage, and functionalization was determined via ^{1}H NMR. Adamantane functionalization of HA was calculated as the area of the ethyl multiplet of adamantane at 1.50-1.85 ppm (12H) relative to the HA backbone at 3.20-4.20 ppm (10H).(24,35) Approximately 20% of the HA repeat units were modified with adamantanes (**Figure S3**). β-cyclodextrin modification of HA was calculated as the area of the hexane linker at 1.35-1.85 ppm (12H) relative to the methyl singlet of HA at 2.1 ppm (3H).(24,35) Approximately 20% of the HA repeat units were modified with β-cyclodextrin (**Figure S4**). CD-HA and Ad-HA were individually dissolved at 6 wt% in PBS containing 0.5 wt% fibers. The two polymer solutions were combined at a 1:1 cyclodextrin to adamantine molar ratio, mixed, centrifuged to remove bubbles, and the hydrogel was transferred into a custom mold. Fibers were aligned within the guest-host hydrogel by applying a magnetic field, as described previously. Mechanical analysis of the guest-host hydrogels, with and without fibers, was performed via rheology (TA Instruments Discovery HR 20). A strain sweep (0.01-100%) and cyclic strain time sweep (alternative periods of low (0.2%) and high (100%) strain) were performed at 37°C using procedures adapted from Loebel, 2017.(24) The crossover strain was 6.3% and 5.3% with and without fibers, respectively (**Figure 1F**). Further, the storage modulus was 1284.6 Pa and 742.5 Pa with and without fibers, respectively. Shear-thinning (G" > G' at high strain) and rapid self-healing (recovery of G' > G" at low strain) behavior was confirmed via a cyclic strain time sweep (**Figure 1G**). Critically, this data indicates the inclusion of fibers did not appear to inhibit crosslinking or the shear-thinning and self-healing behavior of guest-host hydrogels.

View Article Online
DOI: 10.1039/D5TB00694E

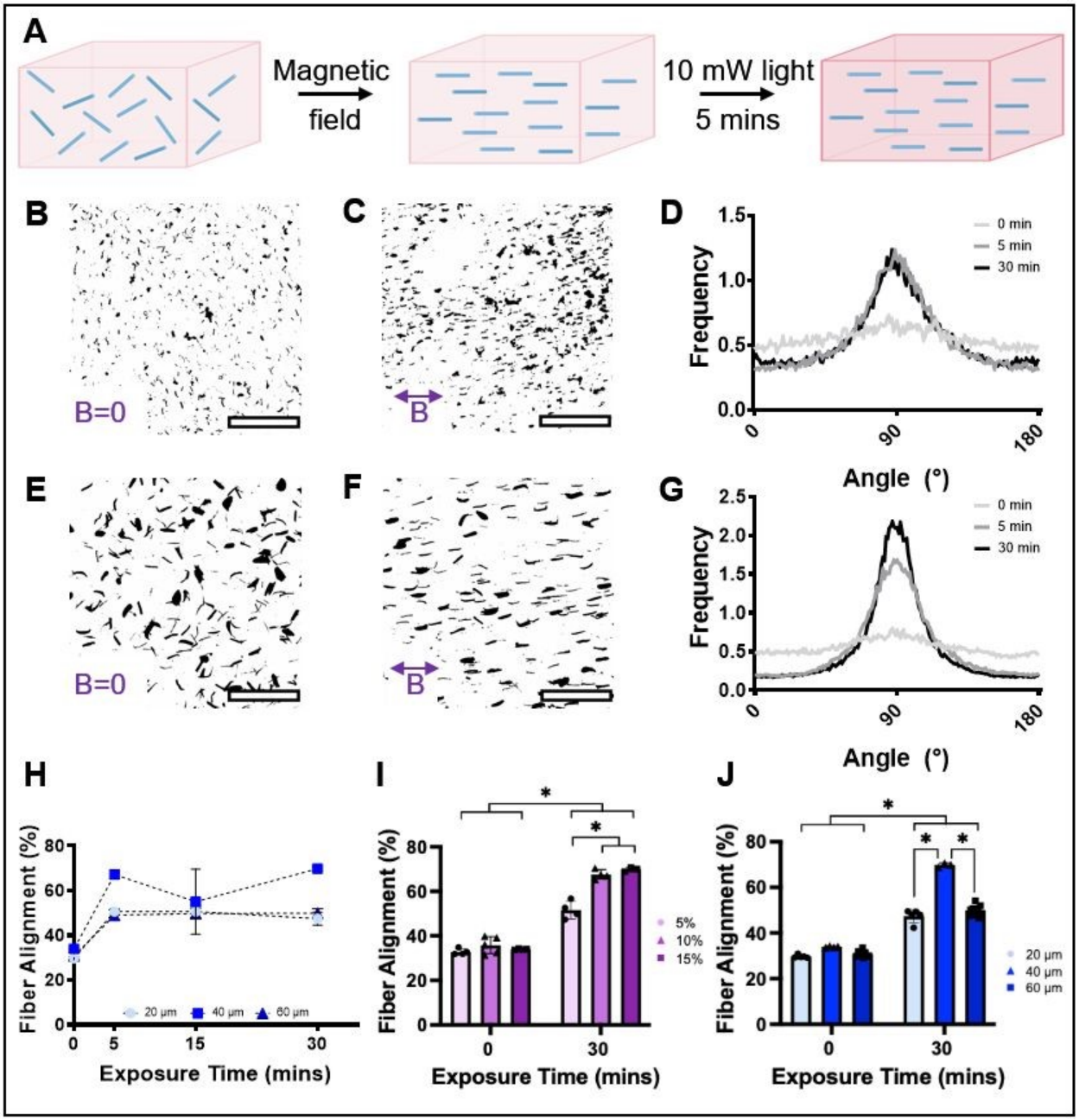

Figure 2. Fibers align rapidly within the polymer solution following magnetic field exposure, where alignment can be locked in place via covalent crosslinking. A) Schematic of the process for fiber alignment within covalently crosslinked hydrogels (created with BioRender.com). Thresholded fluorescent images of 20 µm fibers containing 15% SPIONs within covalently crosslinked hydrogels B) before and C) after magnetic field exposure (620 mT) for 30 minutes. D) Fiber alignment frequency as a function of direction for 20 µm fibers following magnetic field exposure for 0, 5, or 30 minutes. Thresholded fluorescent images of 40 µm fibers containing 15% SPIONs within covalently crosslinked hydrogels E) before and F) after magnetic field exposure (620 mT) for 30 minutes. G) Fiber alignment frequency as a function of direction for 40 µm fibers following magnetic field exposure for 0, 5, or 30 minutes. H) Fiber alignment percent as a function of magnetic field (300 mT) exposure time for 20, 40, and 60 µm fibers. Fiber alignment percent before and after magnetic field exposure (300 mT) for 30 minutes as a function of I) SPION content within 40 µm fibers and J) fiber length with 15% encapsulated SPIONs. Scale bar is 200 µm. B indicates the orientation of the magnetic field.

View Article Online
DOI: 10.1039/D5TB00694E

Following magnetic field exposure, fiber-hydrogel composites were imaged to quantify fiber alignment. Fluorescent images of hydrogels at 10x magnification were processed as follows: deconvolution using CellSens Dimension, thresholding using ImageJ, and then fiber orientation was determined using FiberFit.(36) This data was used to calculate the percentage of fibers aligned in a given direction between 0° to 180° (frequency), where the percent of aligned fibers was defined as the percentage of fibers within ± 25° of the major orientation axis. GraphPad Prism 8 software was used for all statistical analyses. Statistical comparisons were performed using one- or two-way analysis of variance (ANOVA) with Tukey's Honest Significant Difference (HSD) post-hoc testing as appropriate for evaluation of significance between groups ($p<0.05$).

To align fibers within the covalently crosslinked fiber-hydrogel composite **(Figure 2A**), (i) chopped fibers were dispersed within the NorHA polymer solution, (ii) exposed to a magnetic field to induce fiber alignment, and (iii) fiber alignment was locked in place via UV crosslinking. Fiber alignment was locked in place using UV light application while maintaining magnetic field exposure to minimize fiber movement that may occur during magnetic field removal. Fibers were randomly aligned before magnetic field exposure (**Figure 2B, E**) and were highly aligned after magnetic field exposure (**Figure 2C, F**). Generally, fibers containing 15% SPIONs reached maximum fiber alignment in five minutes of magnetic field exposure, where maximum fiber alignment percentage was strongly dependent on fiber length (**Figure 2H, I**). 40 μm fibers aligned more rapidly in the NorHA polymer solution and reached a higher fiber alignment percent compared to 20 or 60 μm fibers. After 30 minutes of magnetic field exposure, fiber alignment percent was 47.5 ± 2.9%, 69.8 ± 0.9%, and 49.9 ± 2.2% for 20, 40, and 60 μm fibers, respectively. This behavior is likely a combination of competing effects: 1) at lower aspect ratios, fibers were more prone to bending, impeding analysis and diminishing the maximum fiber alignment (**Figure S5**) and 2) at high aspect ratios, the forces generated from the magnetic field were insufficient to enable maximum fiber alignment and the fibers were prone to entanglement. Fiber number and area were assessed before (number: 791, area: 336 μm^2) and after 620 mT magnetic field exposure for 30 minutes (number: 801, area: 355 μm^2). No statistical differences were noted before and after magnetic field exposure, which indicates minimal to no fiber aggregation occurred during magnetic field application. Given this data, 40 μm fibers were chosen for subsequent covalently crosslinked fiber-hydrogel studies.

Maximum fiber alignment percent was also strongly dependent on the SPION content within the chopped fibers. Fiber-hydrogel composites with 40 μm fibers containing 10 and 15 wt% SPIONs reached a higher percent alignment than fibers containing 5% SPIONs (**Figure 2J**). Additionally, fibers containing 15% SPIONs achieved peak fiber alignment faster than fibers containing 10% SPIONs (**Figure S6**). Together, this data demonstrates magneto-responsive behavior increased with increasing SPION content, as expected. We were unable to consistently fabricate electrospun fibrous scaffolds with SPION contents above 15 wt%. Thus, 15 wt% SPIONs were used for the rest of this work.

To align fibers within the non-covalently crosslinked fiber-hydrogel composite (**Figure 3A**), the composite was exposed to a magnetic field. The magnetic field application generates a force at the fiber-hydrogel interface. This force was sufficient to locally break (i.e., shear-thin) the non-covalent crosslinks within the hydrogel and enable fiber movement. The non-covalent crosslinks reform after fiber alignment due to the self-healing nature of these bonds. As a result, this platform enables in situ fiber alignment

View Article Online
DOI: 10.1039/D5TB00694E

within the crosslinked hydrogel at any user-defined timepoint. Similar to the covalently crosslinked system, fibers in the non-covalently crosslinked system were randomly aligned before magnetic field exposure (**Figure 3B, E**) and more aligned after magnetic field exposure (**Figure 3C, F**). Fiber alignment was initiated by 30 minutes and increased until 120 minutes of magnetic field exposure (**Figure 3D, G)**. Fiber number and area were assessed before (number: 607, area: 339 μm^2) and after 760 mT magnetic field exposure for 120 minutes (number: 683, area: 346 μm^2). No statistical differences were noted before and after magnetic field exposure, which indicates minimal to no fiber aggregation during magnetic field application.

Generally, fiber alignment within guest-host hydrogels required a longer magnetic field exposure time (>30 mins) and a higher magnetic field strength (760 mT) compared to the covalently crosslinked system. This was expected as the force required to break the non-covalent crosslinks and enable fiber movement is higher than that required within the uncrosslinked NorHA polymer solution. Fiber alignment kinetics (**Figure 3H**) and the maximum fiber alignment percent (**Figure 3I, S7**) were not dependent on fiber length when using a 760 mT magnetic field. 20 and 40 μm fibers reached a maximum fiber alignment of 44.2 ± 2.2% and 43.7 ± 3.2%, respectively. For 40 μm fibers, fiber alignment percent was significantly higher following 120 minutes of exposure to a 760 mT (43.7 ± 3.2%) versus 300 mT (36.9 ± 3.5%) magnetic field (**Figure 3J)**. Interestingly, 20 μm fibers were more aligned than 40 μm fibers following exposure to lower magnetic field strengths (300-620 mT) (**Figure S8**). This behavior is likely due to shorter fibers requiring less force for fiber movement and, thus, a lower magnetic field strength. The alignment of 20 μm fibers was independent of magnetic field strength in the range studied (**Figure S9**). Notably, maximum fiber alignment plateaued at 120 minutes regardless of magnetic field strength and higher exposure times did not increase fiber alignment (**Figure S10**). To maximize fiber alignment, 760 mT was selected for all additional studies using the non-covalently crosslinked system.

View Article Online
DOI: 10.1039/D5TB00694E

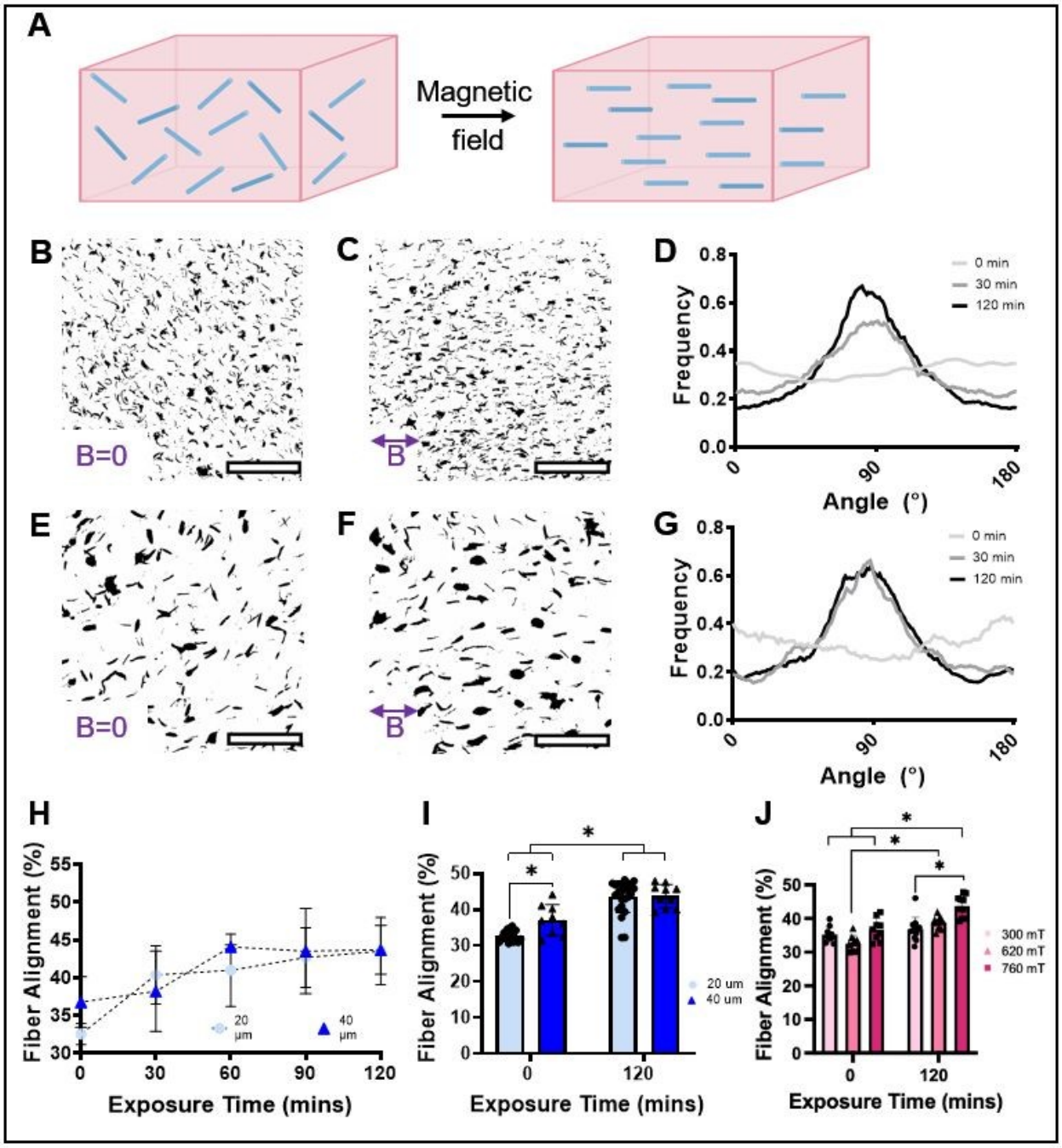

Figure 3. In situ fiber alignment within guest-host hydrogels following magnetic field exposure. A) Schematic of the process for fiber alignment within non-covalently crosslinked hydrogels (created with BioRender.com). Thresholded fluorescent images of 20 μm fibers containing 15% SPIONs within non-covalently crosslinked hydrogels B) before and C) after magnetic field exposure (760 mT) for 120 minutes. D) Fiber alignment frequency as a function of direction for 20 μm fibers following magnetic field exposure for 0, 30, or 120 minutes. Thresholded fluorescent images of 40 μm fibers containing 15% SPIONs within non-covalently crosslinked hydrogels E) before and F) after magnetic field exposure (760 mT) for 120 minutes. G) Fiber alignment frequency as a function of direction for 40 μm fibers following magnetic field exposure for 0, 30, or 120 minutes. H) Fiber alignment percent as a function of magnetic field (760 mT) exposure time for 20 and 40 μm fibers. Fiber alignment percent before and after magnetic field exposure for 120 minutes as a function of I) fiber length with 15% encapsulated SPIONs and J) magnetic field strength for 40 μm fibers. Scale bar is 200 μm. B indicates the orientation of the magnetic field.

View Article Online
DOI: 10.1039/D5TB00694E

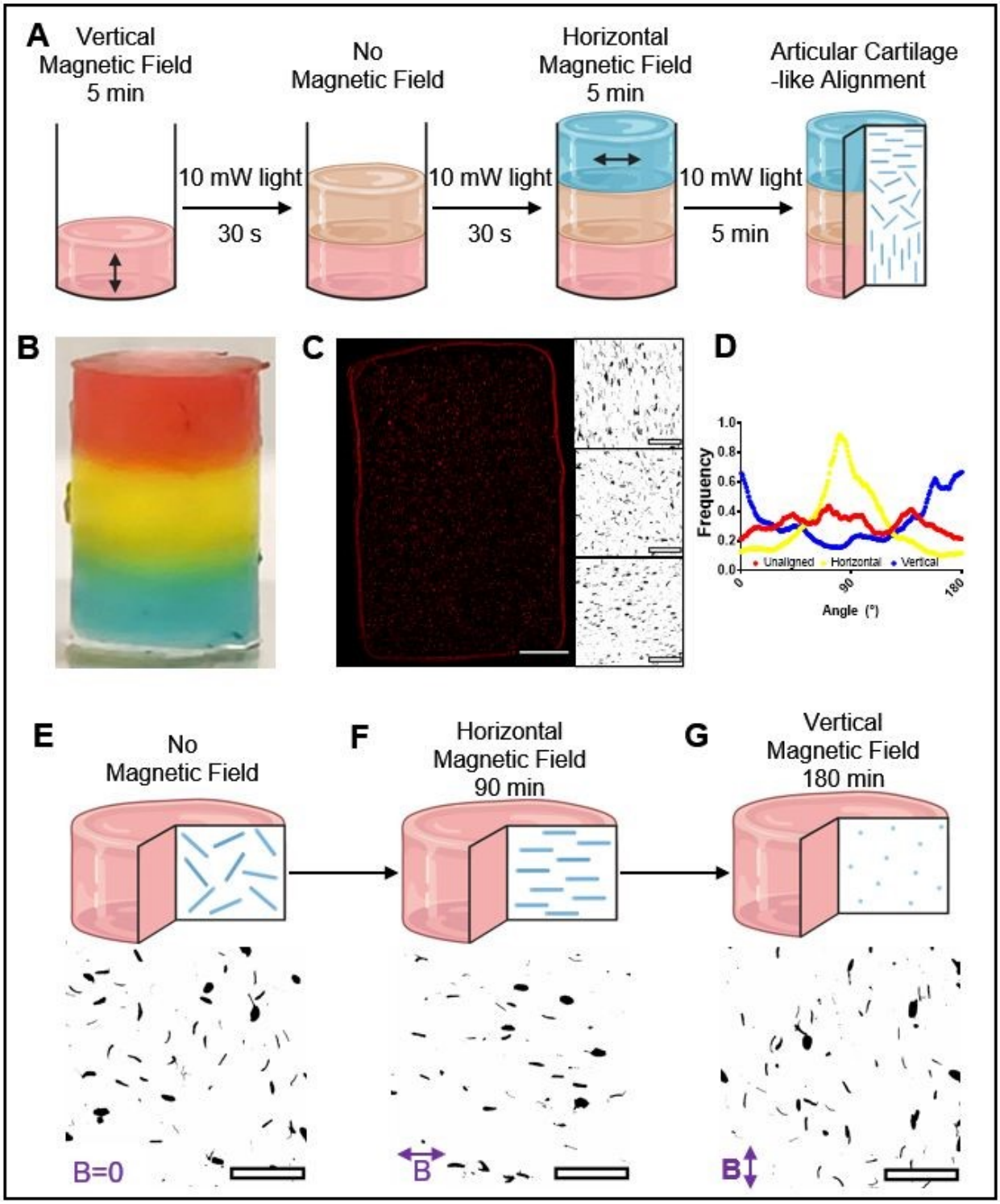

Figure 4. Magnetically-responsive, fiber-hydrogel composites enable spatial and temporal control over 3D fiber alignment. A) Schematic of the process for spatially controlling fiber alignment within covalently crosslinked hydrogels using a layer-by-layer stacking technique. Each layer was exposed to a magnetic field in the desired direction and partially crosslinked to lock alignment in place. At the end, the entire composite was fully crosslinked to generate a robust, multi-layered fiber-hydrogel composite. B) Dye was used to visualize each layer within the tri-layered hydrogel. C) Fluorescent images of the tri-layered hydrogel (scale bar is 1 mm) with magnified images of the fiber alignment within each layer (inset, scale bar is 200 μm). D) Fiber alignment frequency as a function of direction for 40 μm fibers following magnetic field

View Article Online
DOI: 10.1039/D5TB00694E

exposure for each layer. (E-G) Schematic of the process for temporally controlling fiber alignment within non-covalently crosslinked hydrogels: in the same hydrogel at user-defined timepoints fibers were (E) randomly aligned before magnetic field exposure, (F) horizontally aligned after magnetic field exposure in the horizontal direction for 90 minutes, and (G) vertically aligned after magnetic field exposure in the vertical direction for 90 minutes. Scale bar is 200 μm. B indicates the orientation of the magnetic field. (A, E-G created with BioRender.com.)

To enable spatial control over fiber alignment in the covalently crosslinked fiber-hydrogel composite, we used layer-by-layer stacking.(3) Briefly, a layer of uncrosslinked fiber-polymer solution was added to the mold, exposed to a magnetic field, and partially crosslinked using UV light for 30 seconds. This was repeated for each layer, where the direction of the magnetic field can be tuned as desired, and the entire construct was fully crosslinked using UV light for 5 minutes at the end of the process (**Figure 4A**). Partial crosslinking, via UV light exposure for 30 seconds between layers, locks in the fiber alignment while allowing inter-layer diffusion and crosslinking of polymer chains to create a robust, multi-layered hydrogel (**Figure 4B**).(3) This approach allows for the creation of fiber-hydrogel composites that can uniquely mimic the 3D spatial organization of many fibrous tissues, with precise control over both layer depth and the fiber alignment within each layer. Maximum layer thickness is dependent on the penetration depth of UV light, where studies have observed successful UV light penetration up to 6 mm.(37) However, this system can be adapted to crosslink via other wavelengths of light with increased penetration depths. To demonstrate the versatility of this system, fibers were horizontally aligned in the bottom layer, randomly aligned in the middle layer, and vertically aligned in the top layer (**Figure 4C**). A histogram of fiber frequency versus orientation angle demonstrates precise control over fiber orientation within each layer of the hydrogel (**Figure 4D**). The fiber orientation within this composite mimics the 3D spatial organization within the different zones of articular cartilage. In the future, this platform can be used to develop tissue-engineered scaffolds that mimic the complex spatial organization within many connective tissues, such as articular cartilage, and serve as a template for improved repair.

To demonstrate temporal control over fiber alignment in the non-covalently crosslinked fiber-hydrogel composite, we applied a magnetic field with varying magnetic field direction at multiple user-defined timepoints. Critically, due to the shear-thinning and self-healing nature of the guest-host hydrogel, magnetic field exposure was capable of aligning fibers within the crosslinked hydrogel (**Figure 3**). As a proof of concept, fibers were initially randomly aligned before magnetic field exposure (**Figure 4E**). At a user-defined timepoint, fibers were horizontally aligned via magnetic field application in the horizontal direction for 90 minutes (**Figure 4F**). Then, at a second user-defined timepoint, fibers were vertically aligned via magnetic field application in the vertical direction for 90 minutes (**Figure 4G**). For the first time, this study demonstrates in situ temporal control over fiber orientation within crosslinked hydrogels at any user-defined timepoint. As such, this platform can be used to study the temporal role of fiber orientation during development and wound healing.

Conclusions

Here, we successfully fabricated magnetically-responsive, fiber-hydrogel composites which enabled spatial and temporal control over fiber alignment within HA hydrogels following exposure to a magnetic field. Fibers were encapsulated within covalently crosslinked hydrogels and layer-by-layer stacking was used to spatially control fiber orientation. For temporal control, fibers were encapsulated within non-covalently crosslinked, guest-host hydrogels and fiber orientation could be controlled in situ at any

View Article Online
DOI: 10.1039/D5TB00694E

user-defined time point. Fiber alignment kinetics and maximum alignment percent were dependent on hydrogel crosslinking, fiber length, SPION content, and magnetic field exposure. These approaches enable further research into the spatial and temporal role of 3D fiber organization during development, tissue repair, and disease progression.

Acknowledgements
The authors kindly acknowledge funding from the Arizona Biomedical Research Centre (CTR056049). The authors would also like to acknowledge the John M. Cowley Center for High Resolution Electron Microscopy for providing SEM and TEM access, Jordan Yaron for assisting with image analysis, and Gregory Jensen for assisting with polymer synthesis.

Author contributions
Grace Schwarz: Conceptualization, Formal analysis, Investigation, Methodology, Validation, Visualization, Writing – original draft, review & editing. Julianne L. Holloway: Conceptualization, Funding acquisition, Project administration, Resources, Supervision, Writing – review & editing.

Conflicts of interest
There are no conflicts to declare.

Data availability
The data that support the findings of this study are available within this paper, as part of the Supplementary Information, and from the corresponding author upon reasonable request.

View Article Online
DOI: 10.1039/D5TB00694E

References

1. Yang G, Rothrauff BB, Tuan RS. Tendon and Ligament Regeneration and Repair: Clinical Relevance and Developmental Paradigm. Birth Defects Res C Embryo Today. 2013 Sep;99(3):203–22.

2. Petre DG, Leeuwenburgh SCG. The Use of Fibers in Bone Tissue Engineering. Tissue Engineering Part B: Reviews [Internet]. 2022 Feb 15 [cited 2022 Feb 25]; Available from: https://www.liebertpub.com/doi/abs/10.1089/ten.teb.2020.0252

3. Tindell RK, McPhail MJ, Myers CE, Neubauer J, Hintze JM, Lott DG, et al. Trilayered Hydrogel Scaffold for Vocal Fold Tissue Engineering. Biomacromolecules. 2022 Nov 14;23(11):4469–80.

4. Rahmati M, Mills DK, Urbanska AM, Saeb MR, Venugopal JR, Ramakrishna S, et al. Electrospinning for tissue engineering applications. Progress in Materials Science. 2021 Apr 1;117:100721.

5. Kishan AP, Cosgriff-Hernandez EM. Recent advancements in electrospinning design for tissue engineering applications: A review. Journal of Biomedical Materials Research Part A. 2017;105(10):2892–905.

6. Atala A, Irvine DJ, Moses M, Shaunak S. Wound Healing Versus Regeneration: Role of the Tissue Environment in Regenerative Medicine. MRS bulletin / Materials Research Society. 2011 Jan 1;35(8):10.1557/mrs2010.528.

7. Schneider M, Angele P, Järvinen TAH, Docheva D. Rescue plan for Achilles: Therapeutics steering the fate and functions of stem cells in tendon wound healing. Advanced Drug Delivery Reviews. 2018 Apr 1;129:352–75.

8. Li Y, Zhu J, Cheng H, Li G, Cho H, Jiang M, et al. Developments of Advanced Electrospinning Techniques: A Critical Review. Advanced Materials Technologies. 2021;6(11):2100410.

9. Tan GZ, Zhou Y. Electrospinning of biomimetic fibrous scaffolds for tissue engineering: a review. International Journal of Polymeric Materials. 2020 Oct;69(15):947–60.

10. Xie X, Chen Y, Wang X, Xu X, Shen Y, Khan A ur R, et al. Electrospinning nanofiber scaffolds for soft and hard tissue regeneration. Journal of Materials Science & Technology. 2020 Dec 15;59:243–61.

11. Williams MW, Wimberly JA, Stwodah RM, Nguyen J, D'Angelo PA, Tang C. Temperature-Responsive Structurally Colored Fibers via Blend Electrospinning. ACS Appl Polym Mater. 2023 Apr 14;5(4):3065–78.

12. Omidinia-Anarkoli A, Rimal R, Chandorkar Y, Gehlen DB, Rose JC, Rahimi K, et al. Solvent-Induced Nanotopographies of Single Microfibers Regulate Cell Mechanotransduction. ACS Appl Mater Interfaces. 2019 Feb 27;11(8):7671–85.

13. Bou S, Ellis AV, Ebara M. Synthetic stimuli-responsive 'smart' fibers. Current Opinion in Biotechnology. 2016 Jun 1;39:113–9.

View Article Online
DOI: 10.1039/D5TB00694E

14. Omidinia-Anarkoli A, Boesveld S, Tuvshindorj U, Rose JC, Haraszti T, Laporte LD. An Injectable Hybrid Hydrogel with Oriented Short Fibers Induces Unidirectional Growth of Functional Nerve Cells. Small. 2017;13(36):1702207.

15. Teixeira MO, Antunes JC, Felgueiras HP. Recent Advances in Fiber–Hydrogel Composites for Wound Healing and Drug Delivery Systems. Antibiotics. 2021 Mar;10(3):248.

16. Chalard AE, Porritt H, Lam Po Tang EJ, Taberner AJ, Winbo A, Ahmad AM, et al. Dynamic composite hydrogels of gelatin methacryloyl (GelMA) with supramolecular fibers for tissue engineering applications. Biomaterials Advances. 2024 Oct 1;163:213957.

17. Nakielski P, Pawłowska S, Rinoldi C, Ziai Y, De Sio L, Urbanek O, et al. Multifunctional Platform Based on Electrospun Nanofibers and Plasmonic Hydrogel: A Smart Nanostructured Pillow for Near-Infrared Light-Driven Biomedical Applications. ACS Appl Mater Interfaces. 2020 Dec 9;12(49):54328–42.

18. Freeman R, Han M, Álvarez Z, Lewis JA, Wester JR, Stephanopoulos N, et al. Reversible self-assembly of superstructured networks. Science. 2018 Nov 16;362(6416):808–13.

19. Chen T, Bakhshi H, Liu L, Ji J, Agarwal S. Combining 3D Printing with Electrospinning for Rapid Response and Enhanced Designability of Hydrogel Actuators. Advanced Functional Materials. 2018;28(19):1800514.

20. Wang N, Guo F, Wu J, Zhao Y, Jiang L. Variable Responsive Wettability Films via Electrospinning Induced by Solvents. Journal of Nanomaterials. 2014;2014(1):817418.

21. Matera DL, Wang WY, Smith MR, Shikanov A, Baker BM. Fiber Density Modulates Cell Spreading in 3D Interstitial Matrix Mimetics. ACS Biomater Sci Eng. 2019 Jun 10;5(6):2965–75.

22. Patel M, Koh WG. Composite Hydrogel of Methacrylated Hyaluronic Acid and Fragmented Polycaprolactone Nanofiber for Osteogenic Differentiation of Adipose-Derived Stem Cells. Pharmaceutics. 2020 Sep 22;12(9):902.

23. Gramlich WM, Kim IL, Burdick JA. Synthesis and orthogonal photopatterning of hyaluronic acid hydrogels with thiol-norbornene chemistry. Biomaterials. 2013 Dec;34(38):9803–11.

24. Loebel C, Rodell CB, Chen MH, Burdick JA. Shear-thinning and self-healing hydrogels as injectable therapeutics and for 3D-printing. Nat Protoc. 2017 Aug;12(8):1521–41.

25. Ozel F, Kockar H. A Simple Method of Synthesis and Characterizations of Oleate-Coated Iron Oxide Nanoparticles. J Supercond Nov Magn. 2017 Jul 1;30(7):2023–7.

26. Ali A, Zafar H, Zia M, ul Haq I, Phull AR, Ali JS, et al. Synthesis, characterization, applications, and challenges of iron oxide nanoparticles. Nanotechnol Sci Appl. 2016 Aug 19;9:49–67.

27. Bloemen M, Brullot W, Luong TT, Geukens N, Gils A, Verbiest T. Improved functionalization of oleic acid-coated iron oxide nanoparticles for biomedical applications. J Nanopart Res. 2012 Aug 7;14(9):1100.

View Article Online
DOI: 10.1039/D5TB00694E

28. Kuhn J, McDonald A, Mongoin C, Anderson G, Lafeuillade G, Mitchell S, et al. Non-invasive methods of monitoring Fe3O4 magnetic nanoparticle toxicity in human liver HepaRG cells using impedance biosensing and Coherent anti-Stokes Raman spectroscopic (CARS) microscopy. Toxicology Letters. 2024 Apr 1;394:92–101.

29. Buskermolen ABC, Ristori T, Mostert D, van Turnhout MC, Shishvan SS, Loerakker S, et al. Cellular Contact Guidance Emerges from Gap Avoidance. Cell Reports Physical Science. 2020 May 20;1(5):100055.

30. Omidinia-Anarkoli A, Ephraim JW, Rimal R, De Laporte L. Hierarchical fibrous guiding cues at different scales influence linear neurite extension. Acta Biomaterialia. 2020 Sep 1;113:350–9.

31. Licht C, Rose JC, Anarkoli AO, Blondel D, Roccio M, Haraszti T, et al. Synthetic 3D PEG-Anisogel Tailored with Fibronectin Fragments Induce Aligned Nerve Extension. Biomacromolecules. 2019 Oct 31;acs.biomac.9b00891.

32. Pai A, Shetty R, Hodis B, Chowdhury YS. Magnetic Resonance Imaging Physics. In: StatPearls [Internet]. Treasure Island (FL): StatPearls Publishing; 2024 [cited 2024 Jul 10]. Available from: http://www.ncbi.nlm.nih.gov/books/NBK564320/

33. Fumasi FM, MacCulloch T, Bernal-Chanchavac J, Stephanopoulos N, Holloway JL. Using dynamic biomaterials to study the temporal role of bioactive peptides during osteogenesis. Biomaterials advances. 2023 Dec 6;157:213726.

34. Hui E, Gimeno KI, Guan G, Caliari SR. Spatiotemporal Control of Viscoelasticity in Phototunable Hyaluronic Acid Hydrogels. Biomacromolecules. 2019 Oct 22;20(11):4126.

35. Rodell CB, Kaminski A, Burdick JA. Rational Design of Network Properties in Guest-Host Assembled and Shear-Thinning Hyaluronic Acid Hydrogels. Biomacromolecules [Internet]. 2013 Nov 11 [cited 2019 Oct 19];14(11). Available from: https://www.ncbi.nlm.nih.gov/pmc/articles/PMC3851010/

36. Morrill EE, Tulepbergenov AN, Stender CJ, Lamichhane R, Brown RJ, Lujan TJ. A Validated Software Application to Measure Fiber Organization in Soft Tissue. Biomech Model Mechanobiol. 2016 Dec;15(6):1467–78.

37. Lim KS, Klotz BJ, Lindberg GCJ, Melchels FPW, Hooper GJ, Malda J, et al. Visible Light Cross-Linking of Gelatin Hydrogels Offers an Enhanced Cell Microenvironment with Improved Light Penetration Depth. Macromolecular Bioscience. 2019;19(6):1900098.

View Article Online
DOI: 10.1039/D5TB00694E

Data Availability Statement

The data that support the findings of this study are available within this paper, as part of the Supplementary Information, and from the corresponding author upon reasonable request.